

Pacific Shallow Meridional Overturning Circulation in a Warming Climate

DAIWEI WANG* AND MARK A. CANE

Lamont-Doherty Earth Observatory, Columbia University, Palisades, New York

(Manuscript received 24 September 2010, in final form 30 May 2011)

ABSTRACT

By analyzing a set of the Coupled Model Intercomparison Project phase 3 (CMIP3) climate model projections of the twenty-first century, it is found that the shallow meridional overturning of the Pacific subtropical cells (STCs) show contrasting trends between two hemispheres in a warming climate. The strength of STCs and equivalently the STC surface-layer transport tend to be weakening (strengthening) in the Northern (Southern) Hemisphere as a response to large-scale surface wind changes over the tropical Pacific. The STC pycnocline transport convergence into the equatorial Pacific Ocean from higher latitudes shows a robust weakening in the twenty-first century. This weakening is mainly through interior pathways consistent with the relaxation of the zonal pycnocline tilt, whereas the transport change through western boundary pathways is small and not consistent across models. It is found that the change of the western boundary pycnocline transport is strongly affected by the shoaling of the pycnocline base. In addition, there is a robust weakening of the Indonesian Throughflow (ITF) transport in a warming climate. In the multimodel ensemble mean, the response to greenhouse warming of the upper-ocean mass balance associated with the STCs is such that the weakening of the equatorward pycnocline transport convergence is balanced by a weakening of the poleward surface-layer transport divergence and the ITF transport of similar amounts.

1. Introduction

The general circulation of the upper tropical Pacific Ocean is characterized by strong zonal currents and shallow meridional overturning cells (Godfrey et al. 2001; Liu and Philander 2001). Many studies have shown that these cells, known as the subtropical cells (STCs), connect the equatorial thermocline–pycnocline and upwelling regions in the tropics to the subduction regions in the subtropics of both hemispheres, thus providing a principal mechanism for tropical–subtropical water mass exchange (e.g., McCreary and Lu 1994; Liu 1994). The STCs involve waters subducted in the subtropics, flowing equatorward in the pycnocline, feeding into the equatorial undercurrent (EUC), and upwelling in the eastern equatorial regions before returning back to the subtropics in the surface Ekman flow. The equatorward branches of the STCs

in the pycnocline are large-scale geostrophic flows and tend to conserve their potential vorticity (PV). As a result of PV conservation, the pycnocline flows are also oriented westward, reaching the equatorial regions either through the low-latitude western boundary current (LLWBC) or directly in the ocean interior. This basic structure of the STCs has been elucidated by a number of numerical modeling studies (e.g., Liu et al. 1994; Lu et al. 1998; Rothstein et al. 1998; Huang and Liu 1999). The STCs are most prominent in the Pacific Ocean but also found in the Atlantic Ocean (see Schott et al. 2004 for a comprehensive review). In this study, we focus on the Pacific STCs.

Significant decadal variations of the Pacific STCs over the last several decades, particularly the equatorward pycnocline flow in the ocean interior, have been documented based on historical hydrographic data analyses (McPhaden and Zhang 2002, 2004; Zhang and McPhaden 2006). The transport convergence of the equatorward pycnocline flows across 9°N and 9°S in the ocean interior slowed from the 1970s to the 1990s by ~ 13 Sv ($1 \text{ Sv} \equiv 10^6 \text{ m}^3 \text{ s}^{-1}$; McPhaden and Zhang 2002), and thereafter saw a rebound of ~ 11 Sv from 1992–98 to 1998–2003 (McPhaden and Zhang 2004). There was an overall decrease of ~ 11 Sv over the period 1953–2001,

* Current affiliation: Department of Earth, Atmospheric and Planetary Sciences, Massachusetts Institute of Technology, Cambridge, Massachusetts.

Corresponding author address: Daiwei Wang, Lamont-Doherty Earth Observatory, 61 Route 9W, Palisades, NY 10964-8000.
E-mail: dwang@ldeo.columbia.edu

with strong decade-to-decade variations of similar magnitude (Zhang and McPhaden 2006). However, it is unclear how much of this observed long-term trend in the STCs is associated with greenhouse warming. The observed decadal variability and trend of the Pacific STCs have been successfully reproduced by several ocean general circulation model hindcasts forced by historical reanalysis forcing data but with somewhat different magnitudes and weaker-than-observed trends (Lee and Fukumori 2003; Capotondi et al. 2005; Cheng et al. 2007; Lübbecke et al. 2008).

Many studies have suggested an active role of the STCs in modulating the tropical climate and climate variability, particularly on decadal time scales. Since the STCs bring cold pycnocline waters from the subtropics to the tropics and export warm surface waters out of the tropics, they contribute a significant amount of ocean heat transport, thus regulating the upper-ocean heat content in the low latitudes (Klinger and Marotzke 2000; Held 2001). There are two general mechanisms that may make the STCs responsible for the decadal variability in the tropical Pacific. The first mechanism, proposed by Gu and Philander (1997), involves surface temperature anomalies subducted in the subtropics, carried equatorward by the STCs within the pycnocline, before re-emerging in the eastern equatorial upwelling regions, where the anomalies may be amplified through the Bjerknes feedback. The time scales for temperature anomalies to be advected from the subtropics to the tropics are on the order of a decade or two. This mechanism, however, has been called into question for the lack of evidence that these temperature anomalies indeed reach the equatorial regions with discernible amplitude (Schneider et al. 1999; Nonaka and Xie 2000; Hazeleger et al. 2001b).

An alternative mechanism, first proposed by Kleeman et al. (1999), hypothesizes that the decadal variations of the STCs affect the amount of cold pycnocline waters upwelled in the eastern equatorial Pacific, thus creating sea surface temperature (SST) anomalies that may feed back to the surface winds that drive the STCs. This mechanism has gained support from observational analyses showing that the STC interior pycnocline transport convergence is highly correlated with the SST in the central and eastern tropical Pacific on decadal time scales (McPhaden and Zhang 2002, 2004; Zhang and McPhaden 2006). Using an ocean general circulation model forced by observed surface wind stress, Nonaka et al. (2002) found that the off-equatorial winds in the tropics account for about one-half of the decadal SST variability in the eastern equatorial Pacific by spinning up and down the STCs. The strong correlation between the decadal variations of the STCs and tropical SST was also identified in coupled general circulation models (Zhang and McPhaden 2006).

Anthropogenic climate change due to increasing greenhouse gases in the atmosphere has become a principal scientific and socioeconomic concern. The regional signatures of global warming, modulated by natural climate variability and feedback, are rather complex (Xie et al. 2010). A host of robust changes in the tropical Pacific under global warming have been identified in climate projection simulations by state-of-the-art coupled general circulation models (Vecchi et al. 2006; Vecchi and Soden 2007; DiNezio et al. 2009). The changes include a weakening of the Walker circulation and associated easterly trade winds, a shoaling and intensification of the equatorial thermocline, a weakening of the surface zonal currents, and a reduction of the Indonesian Throughflow (ITF). With a few exceptions, however, little work has focused on the possible response of the STCs to future greenhouse warming. Merryfield and Boer (2005) analyzed three anthropogenically forced warming simulations of the Canadian Centre for Climate Modelling and Analysis (CCCma) global coupled model from 1900 to 2100 and found the simulated STC pycnocline transports in the ocean interior decrease progressively under global warming in both hemispheres with a reduction up to 46% by 2100 (their Fig. 2). Lohmann and Latif (2005) analyzed a 240-yr greenhouse warming scenario integration from the coupled ECHAM4/Ocean Isopycnal Model (OPYC) and found the STC strength, measured by the meridional overturning streamfunction, is decreasing (increasing) in the Northern (Southern) Hemisphere (their Fig. 13). A similar result was noted by Park et al. (2009) in their global warming simulations of a different coupled model, the Kiel Climate Model (their Fig. 13). These studies are all based on one single model, leaving the question of whether their results are model dependent or not. The only multimodel intercomparison study that we are aware of is Luo et al. (2009), who analyzed an ensemble of 11 coupled global climate models and found the interior (western boundary) STC pycnocline transport is reduced (enhanced) in a warmer period 2151–2200 relative to a present-day period 1951–2000 in most models, resulting in no significant change of the total STC transport. This result, however, is at odds with our analysis, and the discrepancy will be discussed in section 3d.

The partitioning of the STC transport between the interior and the western boundary regions has been a topic of particular interest. A number of modeling studies showed that there is a partial compensation of the STC transport variations between the interior and western boundary regions on interannual-to-decadal time scales. Lee and Fukumori (2003) found in their model that the variation of STC western boundary transport is out-of-phase with and smaller than that of the STC interior transport. They attributed this partial compensation to

TABLE 1. CMIP3 models analyzed in this study. Horizontal resolution is expressed as degree longitude by latitude (with enhanced latitudinal spacing in the parentheses). Vertical resolution, starting with the letter L, is the number of vertical levels.

Model ID	Model name	Country	Ocean resolution	Reference
1	CGCM3.1(T47)	Canada	$1.85^{\circ} \times 1.85^{\circ}$ L29	Kim et al. (2002)
2	CGCM3.1(T63)	Canada	$1.4^{\circ} \times 0.94^{\circ}$ L29	Kim et al. (2002)
3	CSIRO Mk3.0	Australia	$1.875^{\circ} \times 0.84^{\circ}$ L31	Gordon et al. (2002)
4	CSIRO Mk3.5	Australia	$1.875^{\circ} \times 0.84^{\circ}$ L31	Gordon et al. (2002)
5	GFDL CM2.0	United States	$1^{\circ} \times 1^{\circ}(1/3^{\circ})$ L50	Delworth et al. (2006)
6	GFDL CM2.1	United States	$1^{\circ} \times 1^{\circ}(1/3^{\circ})$ L50	Delworth et al. (2006)
7	MRI CGCM2.3.2	Japan	$2.5^{\circ} \times 2^{\circ}(0.5^{\circ})$ L23	Yukimoto and Noda (2002)

the covariability of off-equatorial wind stress curl in the western Pacific and near-equatorial zonal wind stress. Capotondi et al. (2005) also found in a different ocean model that the STC boundary transport variation tends to partially compensate for the interior transport variation, which they argued is a consequence of the baroclinic adjustment to large-scale wind stress curl variations. Lübbecke et al. (2008), however, suggested that the compensatory variations of the STC interior and western boundary transports are a result of wind-driven expansion and contraction of the poleward extent of the tropical gyres. It is unclear, however, whether this compensatory behavior is also present on longer time scales associated with greenhouse warming.

In this study, we analyzed the projected long-term change of the Pacific STCs in the twenty-first century simulated by a coordinated suite of coupled general circulation models. Section 2 details the model output data that we analyzed and the diagnostic methods that we used. In section 3, we present the results in terms of the changes of the meridional overturning streamfunction, the surface-layer transport and the pycnocline transport of the Pacific STCs, as well as the Indonesian Throughflow transport. Section 4 concludes the paper with a summary and discussion of our main findings.

2. Data and methods

We analyzed a coordinated suite of twenty-first century climate projections from the World Climate Research Programme (WCRP) Coupled Model Intercomparison Project phase 3 (CMIP3) multimodel dataset that serves the Intergovernmental Panel on Climate Change (IPCC) Fourth Assessment Report (AR4; Meehl et al. 2007). The projections are based on the numerical simulations of state-of-the-art global climate models subject to the radiative forcing of the Special Report on Emission Scenarios (SRES) A1B, in which the atmospheric CO_2 concentration, among other greenhouse gases, ramps from the present-day level to 720 ppm by year 2100. The model output data of ocean, atmosphere, and land surface variables from 25 climate models are archived at

and made available by the Program for Climate Model Diagnosis and Intercomparison (PCMDI). Since our goal is to analyze the meridional overturning circulation in the tropical Pacific Ocean, we used the three-dimensional ocean meridional velocity fields from seven CMIP3 models, whose names and specifications are listed in Table 1. This small subset of models was chosen among the total 25 models because their ocean velocity fields are archived on the original model grids, thus preserving mass balance closure. We examined the mass balance closure in each model in the following way. The mean meridional velocity is integrated vertically from surface to bottom and zonally around the globe. If mass is conserved, the resultant meridional transport should be exactly zero if the model uses a rigid-lid formulation or near zero if the model uses a free surface formulation. It was found, however, this transport is on the order of several Sv or even larger in the majority of the models, suggesting considerable errors in their meridional mass transport. Therefore we excluded all the models whose global mean meridional transport exceeds 1 Sv in magnitude. We used the ocean potential density fields from the same models to determine the base of the tropical pycnocline that marks the lower boundary of the equatorward pycnocline flow. In addition, the zonal and meridional surface wind stress fields are used to compute the wind-driven meridional transport so as to compare with the actual transport derived from the ocean meridional velocity. It is worth mentioning that among seven selected models, CCCma Coupled General Circulation Model, version 3.1 (CGCM3.1) (T47) and CGCM3.1 (T63) are essentially the same model of different resolutions; Commonwealth Scientific and Industrial Research Organisation Mark version 3.0 (CSIRO Mk3.0) and CSIRO Mk3.5 share the same horizontal and vertical resolution but have significant differences in model physical parameterizations; the Geophysical Fluid Dynamics Laboratory Climate Model version 2.0 (GFDL CM2.0) and GFDL CM2.1 also have approximately the same resolution but differ in the numerics of atmospheric dynamical core and in the parameter settings for some of the oceanic subgrid-scale physics.

The meridional overturning circulation in the ocean is commonly represented by the meridional overturning streamfunction as a function of latitude, depth, and time

$$\Psi(\phi, z, t) = \int_z^0 \int_{\lambda_W}^{\lambda_E} v(\lambda, \phi, z, t) a \cos\phi \lambda \, dz, \quad (1)$$

where $a = 6370$ km is the radius of the earth, v is meridional velocity as a function of longitude λ , latitude ϕ , depth z , and time t . Here, λ_E and λ_W are the longitudes of the eastern and western boundary of an ocean basin, respectively. In the tropical Pacific Ocean, λ_E marks the west coast of the American continent. In the western tropical basin, the Pacific Ocean is connected to the Indian Ocean through several Indonesian sea passages. The λ_W denotes the east coast of East and Southeast Asia in the Northern Hemisphere and the east coast of Australia–New Guinea in the Southern Hemisphere, with the equator separating the Pacific Ocean and the Indian Ocean in the vicinity of Indonesian Seas. In addition, the Torres Strait between Australia and New Guinea is open with a finite transport in three models [CSIRO Mk3.0, CSIRO Mk3.5, and the Meteorological Research Institute Coupled General Circulation Model, version 2.3.2 (MRI CGCM2.3.2)]. The meridional overturning streamfunction in these models is thus left undefined near 10°S where the Torres Strait is located.

To quantify the water mass exchange between the tropics and subtropics, it is common practice to compute the zonally and vertically integrated poleward surface transport and equatorward pycnocline transport along specific latitudes. We chose to compute these meridional transports along 9°N and 9°S, following most of the previous studies (e.g., McPhaden and Zhang 2002, 2004; Capotondi et al. 2005; Zhang and McPhaden 2006; Luo et al. 2009). These latitudes are poleward of the meridional extent of the tropical cells (about 5°S–5°N) and equatorward of the bifurcation latitudes of the North and South Equatorial Currents (about 15°N and 15°S). To compute the poleward surface transport, the meridional velocity is first integrated zonally from the western boundary to the eastern boundary of the Pacific Ocean along 9°N and 9°S, then vertically from the surface to the depth where the zonally integrated flow turns from poleward to equatorward. This depth marks the base of the surface layer and is about 50 m. The equatorward pycnocline transport is vertically integrated from the base of the surface layer to the base of the pycnocline and divided into two components: the interior pycnocline transport and the western boundary pycnocline transport. The former is zonally integrated from the dividing longitude between the interior and western boundary regimes to the eastern boundary; the latter

from the western boundary to the dividing longitude, which is 135°E at 9°N and 160°E at 9°S near the east edge of the LLWBC and its recirculation. The choice of dividing longitudes is consistent with previous studies (Lee and Fukumori 2003; Capotondi et al. 2005). The sum of two transport components gives the total pycnocline transport across 9°N and 9°S.

The determination of the pycnocline base as the lower boundary of the equatorward pycnocline transport is somewhat involved. Previous studies chose to integrate the meridional pycnocline transport above a specific isopycnal surface, for example, 26 (26.2) kg m⁻³ along 9°N (S) in McPhaden and Zhang (2002), 26 kg m⁻³ along both 9°N and 9°S in Capotondi et al. (2005), and 26.5 kg m⁻³ along both 10°N and 10°S in Lee and Fukumori (2003). In our multimodel climate change analysis, however, the representative isopycnal surface for the tropical pycnocline base varies from model to model and also changes over time as seawater becomes less dense under greenhouse warming. Therefore, we adopted the functional definition of the tropical pycnocline base of Johnson and McPhaden (1999) as the isopycnal surface at which the interior meridional transport changes sign from equatorward above to poleward below. Specifically, the meridional velocity is first interpolated from depth coordinate to potential density coordinate, before being zonally integrated from the dividing longitude to the eastern boundary along 9°N and 9°S. From the resultant interior meridional transport in potential density coordinate, time-varying turning density is located as the pycnocline base where the flow is equatorward above (except in the lowest density classes where the surface flow is poleward) and poleward below. To ensure that turning density is always found in the upper ocean for every single year, a 3-yr running averaging is applied to the interior meridional transport in potential density coordinate. The pycnocline base determined with this procedure differs from model to model and to a lesser degree between 9°N and 9°S. It also becomes less dense with time in the twenty-first century (Fig. 1).

Not all equatorward flow in the pycnocline that converges across 9°N and 9°S reaches the Pacific equatorial pycnocline. Part of it leaks out into the Indian Ocean through the Indonesian seas. Since the meridional flow in the ITF is mostly southward in the upper ocean, there is no turning density or depth. Therefore, we defined the pycnocline base in the ITF region as the surface of the averaged potential density of the pycnocline base at 9°N and 9°S. The ITF transport is computed as the vertically integrated meridional transport between the surface and pycnocline base at 4°S across all ITF passages.

In addition to various meridional transports derived directly from the ocean meridional velocity field as described,

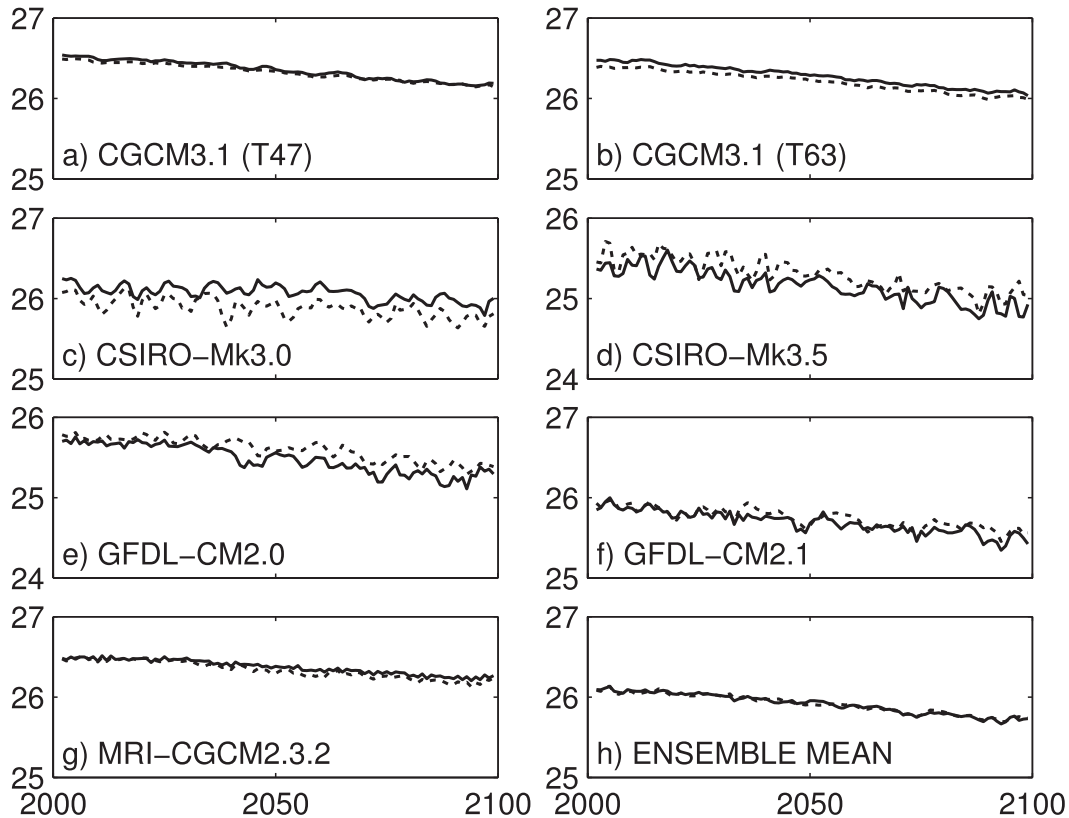


FIG. 1. Time series of the potential density (kg m^{-3}) at the base of the pycnocline in the twenty-first century at 9°N (solid) and 9°S (dotted) for (a)–(g) individual CMIP3 models and (h) the multimodel ensemble mean.

we also computed the zonally integrated meridional Ekman transport based on Ekman theory and the zonally integrated meridional geostrophic transport based on Sverdrup theory for comparison. The Ekman transport per unit longitude is given by

$$M_e = -\frac{\tau^x}{\rho_0 f}, \quad (2)$$

where τ^x is the zonal component of surface wind stress, f is the Coriolis parameter, and ρ_0 is the reference density of seawater. Equation (2) was zonally integrated from the western boundary to the eastern boundary of the Pacific along 9°N and 9°S . The geostrophic transport per unit longitude based on Sverdrup theory is given by

$$M_g = \frac{\text{curl } \tau}{\rho_0 \beta} + \frac{\tau^x}{\rho_0 f}, \quad (3)$$

where $\text{curl } \tau$ is the surface wind stress curl, and β is the meridional derivative of the Coriolis parameter f . Equation (3) was zonally integrated from the dividing longitude to the eastern boundary of the Pacific along 9°N and 9°S .

The archived monthly model data at PCMDI were averaged into yearly means for all the analyses in this paper. The projected change in any meridional transport was computed as the linear least squares trend in the yearly transport time series over the twenty-first century, with the 95% confidence interval obtained by the F test. A trend is considered as statistically “significant” if the p value is less than 0.05 (statistically significant at the 95% confidence level), as “marginally significant” if the p value falls between 0.05 and 0.1 (statistically significant at the 90% but not 95% confidence level), and as “not significant” if the p value is larger than 0.1. The sign convention is such that a transport, as discussed in sections 3b–e, is always positive in its prevailing direction, which means that a strengthening (weakening) transport trend is always positive (negative).

3. Results

a. Shallow meridional overturning circulation

Figure 2 shows the mean meridional overturning streamfunction Ψ averaged over the first 20 years of the twenty-first century (contours) and linear trend of Ψ

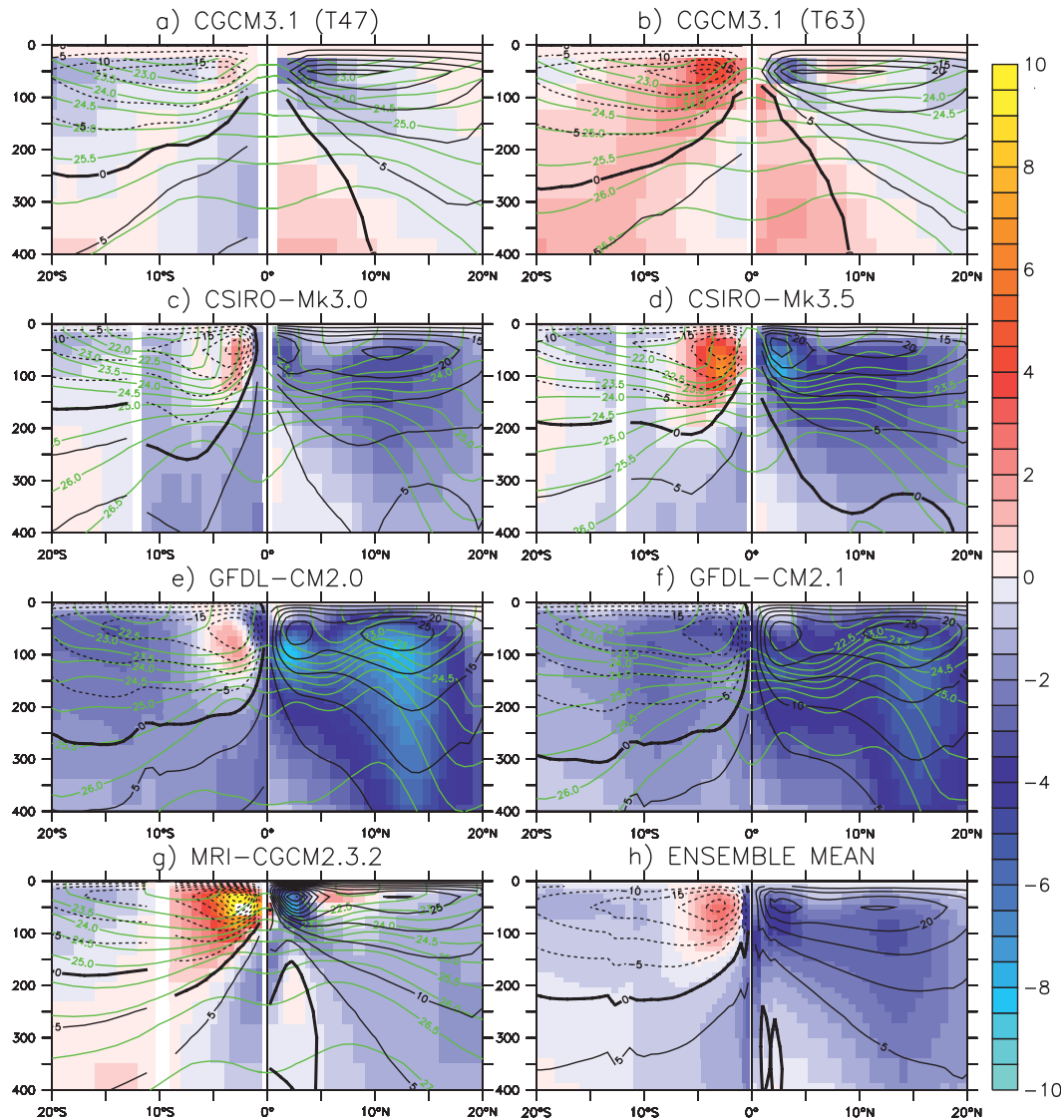


FIG. 2. Linear least squares trends of the meridional overturning streamfunction Ψ in the Pacific between 20°N and 20°S in the twenty-first century (shading, Sv century^{-1}) with the time-mean Ψ averaged over the first 20 years of the twenty-first century (black contours, Sv) for (a)–(g) individual CMIP3 models and (h) the multimodel ensemble mean. Also shown is the time-mean potential density in the central Pacific (160°W) averaged over the first 20 years of the twenty-first century (green contours, kg m^{-3}).

over the twenty-first century (shading) in the upper Pacific Ocean between 20°S and 20°N for each individual model and their ensemble mean. The mean structure of the STCs on both sides of the equator is captured reasonably well by the models. The turning depth between the poleward surface flow and the equatorward pycnocline flow where Ψ reaches local extrema is at about 50 m. The strength of the STC overturning, outside the equatorial region, is about 15–25 Sv in both hemispheres. Near the equator between 5°S and 5°N , there is stronger overturning on both sides of the equator. These equatorially confined tropical cells (TCs) are thought not to

be involved in the subtropical–tropical water mass exchange (Hazeleger et al. 2001a).

Next we examine the projected change of the STC meridional overturning streamfunction in the twenty-first century. In the Northern Hemisphere, the STC overturning shows consistent weakening trends in four models (CSIRO Mk3.0, CSIRO Mk3.5, GFDL CM2.0, and GFDL CM2.1), while the change is less obvious in the other three models. The change of the STC overturning in the Southern Hemisphere is less consistent across models. Strengthening trends are seen in CGCM3.1(T47), CSIRO Mk3.0, GFDL CM2.0, and GFDL CM2.1, while

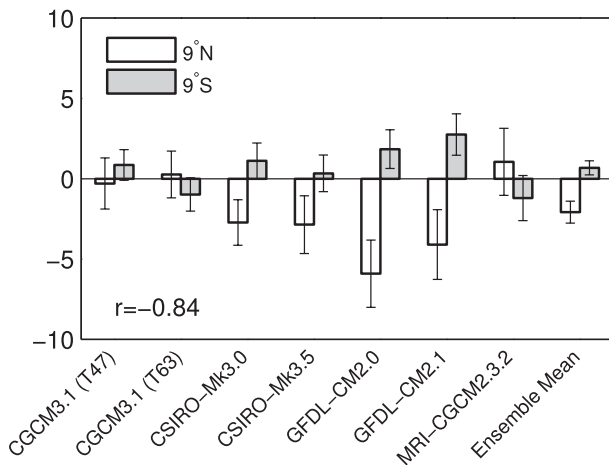


FIG. 3. Linear least squares trends (Sv century^{-1}) of the surface-layer transport in the twenty-first century across 9°N and 9°S for individual CMIP3 models and the multimodel ensemble mean. Positive (negative) values indicate strengthening (weakening) trends. Error bars indicate the 95% confidence intervals for the trends based on the F test.

weakening trends are found in CGCM3.1(T63). The change is less clear in CSIRO Mk3.5 and MRI CGCM2.3.2. In summary, the twenty-first century climate projections show a consistent weakening of the STC overturning in the Northern Hemisphere, while the Southern Hemisphere STC tends to strengthen (to become more negative) in most but not all models. This is reflected in the trends of the ensemble-mean meridional overturning streamfunction averaged across all seven models as follows (Fig. 2h): the northern STC weakens (a negative trend on a positive mean) while the southern STC strengthens slightly (a weak negative trend added to a negative mean), and the TC overturning between 5°S and 5°N shows robust weakening trends in both hemispheres.

b. Surface-layer meridional transport

The meridional overturning streamfunction gives a general picture of the shallow meridional overturning associated with the STCs. In addition, we analyzed the twenty-first-century changes in the individual branches of the STCs as they may not all respond to greenhouse warming in the same fashion. The linear trends of the meridional surface-layer transport—the poleward branch of the STCs—are shown in Fig. 3. The surface-layer transport across 9°N exhibits a general weakening. The weakening trends are statistically significant in four models (CSIRO Mk3.0, CSIRO Mk3.5, GFDL CM2.0, and GFDL CM2.1) but not in the other three models. The weakening trend in the ensemble-mean surface-layer transport across 9°N is $-2.1 \pm 0.7 \text{ Sv century}^{-1}$. In the Southern Hemisphere, the surface-layer transport across

9°S shows some strengthening but is less robust across models. The strengthening trends are statistically significant in two models (GFDL CM2.0 and GFDL CM2.1) and marginally significant in another two models [CGCM3.1(T47) and CSIRO Mk3.0], whereas in CGCM3.1(T63) and MRI CGCM2.3.2 we find marginally significant weakening trends. The strengthening trend in the ensemble-mean surface-layer transport across 9°S is $0.7 \pm 0.4 \text{ Sv century}^{-1}$. It is evident that the surface-layer transport changes tend to be contrasting between two hemispheres: weakening across 9°N and strengthening across 9°S . Indeed, there is a strong negative intermodel correlation ($r = -0.84$, where r is the intermodel correlation coefficient) between the trends of the surface-layer transport across 9°N and 9°S . As a result of this partial compensation of the interhemispheric contrasting changes in the meridional surface-layer transport, the change of the surface-layer transport divergence across 9°N and 9°S is less consistent across models (Table 2). A general weakening is evident, but the weakening trends are statistically significant in only three models (CSIRO Mk3.0, CSIRO Mk3.5, and GFDL CM2.0). The multimodel ensemble-mean surface-layer transport divergence has a weakening trend of $-1.4 \pm 0.8 \text{ Sv century}^{-1}$.

The contrasting and correlated changes in the meridional surface-layer transport across 9°N and 9°S are intriguing and require explanation. In principle, the meridional flow near the ocean surface is largely driven by the zonal component of the surface wind stress through Ekman dynamics. A change in the zonal wind stress will alter the Ekman transport and subsequently the meridional transport in the surface layer. So we compared the twenty-first century changes in the meridional Ekman transport and the surface-layer transport, which are highly correlated at both 9°N and 9°S (Fig. 4). The extremely strong correlations ($r = 0.99$) indicate that the interhemispheric contrasting trends in the meridional surface transport are predominantly driven by the weakening (strengthening) of the off-equatorial easterlies along 9°N (S) through Ekman dynamics. It is noteworthy that the slope of the intermodel linear fit is less than 1 at both latitudes. This is because the changes in the ageostrophic Ekman transport are partially compensated by the changes in the geostrophic transport in the surface layer.

We further examined the large-scale patterns of the surface wind stress change responsible for the contrasting trends in the meridional surface-layer transport across 9°N and 9°S . Figure 5 shows the multimodel ensemble-mean linear trends in the zonal wind stress τ^x over the tropical Pacific in the twenty-first century averaged across all seven models. In the equatorial region (about 5°S – 5°N), the easterly trade winds weaken under global warming, noted in a number of previous studies and

TABLE 2. The linear least squares trends (Sv century⁻¹) of various transport time series associated with the STCs in the twenty-first century for individual CMIP3 models and their ensemble mean. Here, V_S is the surface-layer transport divergence across 9°N and 9°S; V_{IP} , V_{BP} , and V_P are the interior, western boundary, and total pycnocline transport convergence across 9°N and 9°S; V_{ITF} is the ITF transport above the pycnocline base across 4°S; and V_R is the vertical transport across the pycnocline base computed as the residual of V_S , V_P , and V_{ITF} . Positive (negative) values indicate strengthening (weakening) trends. Errors indicate the 95% confidence intervals for the trends based on the F test.

Model name	V_S	V_{IP}	V_{BP}	V_P	V_{ITF}	V_R
CGCM3.1(T47)	0.6 ± 1.8	-2.5 ± 1.5	0.6 ± 0.8	-1.9 ± 1.4	-2.3 ± 0.5	0.2 ± 1.8
CGCM3.1(T63)	-0.7 ± 1.7	-3.1 ± 1.6	0.1 ± 1.0	-3.0 ± 1.4	-1.8 ± 0.5	0.5 ± 1.7
CSIRO Mk3.0	-1.6 ± 1.6	-0.6 ± 2.1	-1.2 ± 1.5	-1.7 ± 2.4	-1.8 ± 0.6	-1.7 ± 2.6
CSIRO Mk3.5	-2.5 ± 2.3	-5.0 ± 2.9	1.7 ± 1.9	-3.3 ± 1.9	-1.8 ± 0.6	-1.0 ± 3.3
GFDL CM2.0	-4.1 ± 2.6	-7.0 ± 2.9	0.2 ± 1.8	-6.8 ± 2.2	-1.4 ± 0.6	1.3 ± 3.6
GFDL CM2.1	-1.3 ± 2.4	0.1 ± 3.2	-1.9 ± 2.5	-1.9 ± 2.3	-0.2 ± 0.7	0.3 ± 3.4
MRI CGCM2.3.2	-0.2 ± 2.0	-6.2 ± 3.2	4.2 ± 2.0	-2.0 ± 2.4	-1.0 ± 0.7	0.8 ± 2.5
Ensemble mean	-1.4 ± 0.8	-3.5 ± 1.0	0.5 ± 0.7	-2.9 ± 0.8	-1.5 ± 0.2	0.1 ± 1.0

linked to the weakening of the Walker circulation driven by changes in the atmospheric hydrological cycle in response to greenhouse warming (Held and Soden 2006; Vecchi et al. 2006; Vecchi and Soden 2007). The weakening of the equatorial trade winds explains the slowdown of the TCs. The largest changes of τ^x , however, are found outside the equatorial region. The trends of the off-equatorial τ^x exhibit a striking spatial pattern of interhemispheric asymmetry. Specifically, τ^x weakens in the Northern Hemisphere west of 120°W between 5°N and 20°N with the maximum weakening trend up to 0.1 dPa century⁻¹ near the location of the mean northeast trade wind maximum (~1.0 dPa) in the central

Pacific. East of 120°W, there is a modest strengthening of τ^x where the mean easterlies are weak. On the contrary, τ^x strengthens almost everywhere over the tropical South Pacific (south of 5°S) except in the far east. The maximum strengthening trend of about -0.1 dPa century⁻¹ is found to the west of the mean southeast trade wind maximum (~0.6 dPa) in the southeastern Pacific. The large-scale, coherent changes in the off-equatorial trade winds over the tropical Pacific of opposite signs between two hemispheres thus explain the inter-hemispherically contrasting changes in the meridional surface-layer transport over a broad latitudinal range in the off-equatorial tropics through Ekman dynamics. In

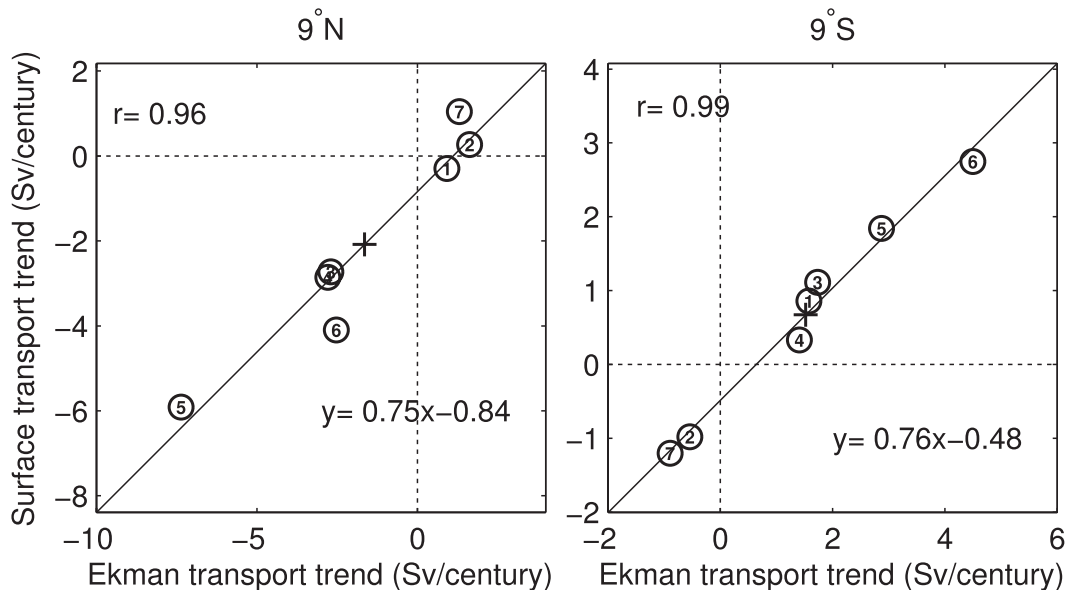


FIG. 4. Intermodel scatterplot and linear fit of the linear least squares trends in the meridional Ekman transport and surface-layer transport across 9°N and 9°S, respectively. Each open circle denotes a CMIP3 model marked by its model ID; the cross denotes the multimodel ensemble mean. Also shown are intermodel correlation coefficient and regression equation.

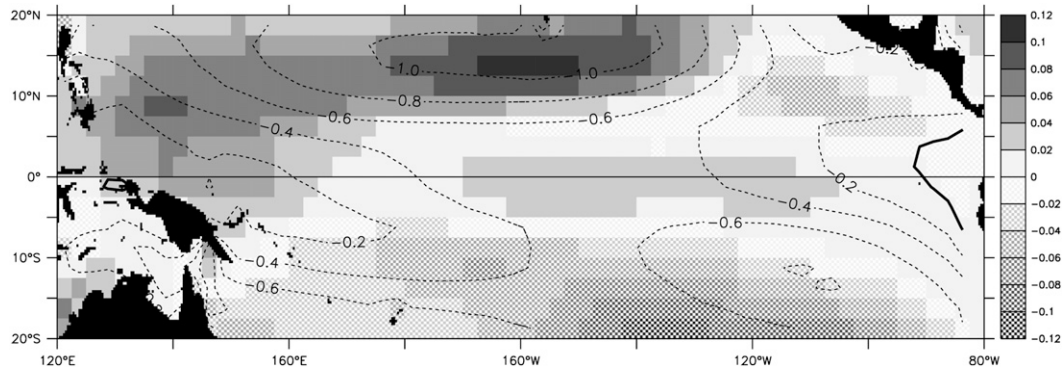


FIG. 5. Linear least squares trends of the multimodel ensemble-mean zonal wind stress in the twenty-first century over the tropical Pacific (dPa century^{-1}). Overlying contours are the mean multimodel ensemble-mean zonal wind stress over the first 20 years of the twenty-first century (in dPa).

addition, the convergence of the surface wind stress under the ITCZ shows a robust weakening across all models (not shown).

c. Interior pycnocline meridional transport

Unlike the surface-layer transport, the interior pycnocline transport across 9°N and 9°S tends to weaken in both hemispheres (Fig. 6). The interior pycnocline transport across 9°N shows significant weakening trends in three models [CGCM3.1(T47), CSIRO Mk3.5, and GFDL CM2.0] and a marginally significant weakening trend in CGCM3.1(T63). The multimodel ensemble-mean trend in the interior pycnocline transport across 9°N is $-1.2 \pm 0.4 \text{ Sv century}^{-1}$. In the Southern Hemisphere, the weakening of the interior pycnocline transport across 9°S is more robust than in the Northern Hemisphere. The weakening trends are significant in four models [CGCM3.1(T63), CSIRO Mk3.5, GFDL CM2.0, and MRI CGCM2.3.2]. The trend in the multimodel ensemble-mean interior pycnocline transport across 9°S is $-2.3 \pm 0.7 \text{ Sv century}^{-1}$. Because the interior pycnocline transport tends to weaken in both hemispheres, the pycnocline transport convergence in the ocean interior across both 9°N and 9°S shows robust weakening trends in most models, with the weakening significant in five models [CGCM3.1(T47), CGCM3.1(T63), CSIRO Mk3.5, GFDL CM2.0, and MRI CGCM2.3.2; see Table 2]. In terms of the multimodel ensemble mean, the interior pycnocline transport convergence weakens by $3.5 \pm 1.0 \text{ Sv}$ in the twenty-first century.

What accounts for the projected weakening of the pycnocline transport in the ocean interior? Since large-scale pycnocline flow in the ocean interior is essentially geostrophic, we first compared the changes in the interior pycnocline transport convergence across both 9°N and 9°S and the geostrophic transport convergence based on Sverdrup theory across the same latitudes. Figure 7

shows that there is a very strong intermodel correlation ($r = 0.96$) between the two, suggesting that the intermodel spread in the interior pycnocline transport change stems from the differences in the local zonal wind stress and wind stress curl via Sverdrup dynamics. Sverdrup theory, however, does not explain the robust weakening of the interior pycnocline transport in most models because the geostrophic transport convergence shows both weakening and strengthening trends across models. This discrepancy is not unexpected as the geostrophic transport based on Sverdrup theory measures the geostrophic flow integrated over the entire water column rather than the pycnocline alone. It also suggests that the weakening of the interior pycnocline transport is associated with the changes in the vertical structure of the geostrophic flow,

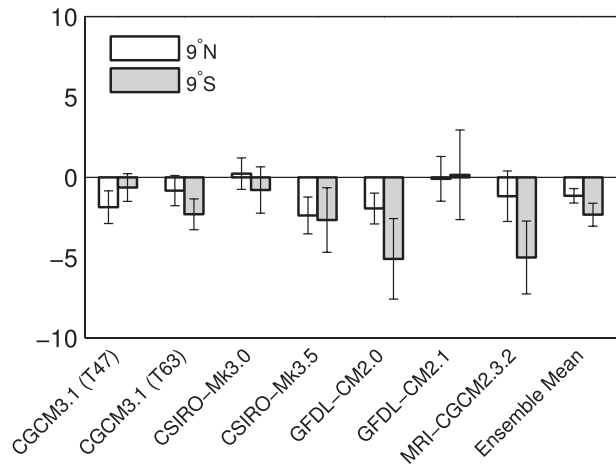


FIG. 6. Linear least squares trends (Sv century^{-1}) of the interior pycnocline transport in the twenty-first century across 9°N and 9°S for individual CMIP3 models and the multimodel ensemble mean. Positive (negative) values indicate strengthening (weakening) trends. Error bars indicate the 95% confidence intervals for the trends based on the F test.

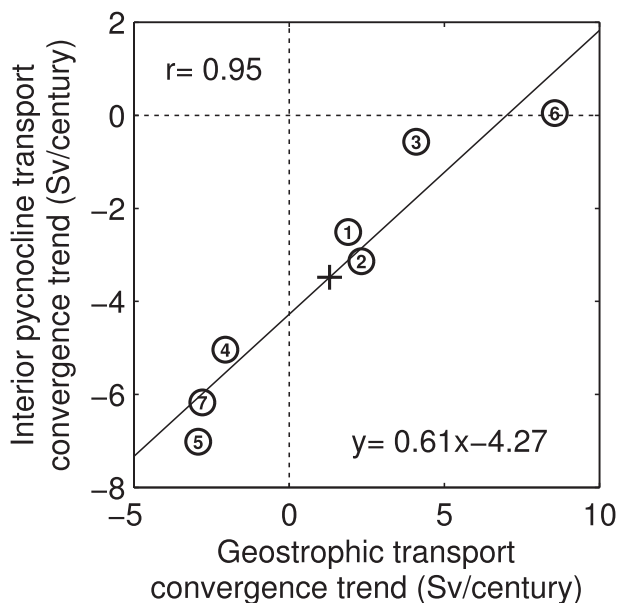


FIG. 7. Intermodel scatterplot and linear fit of the linear least squares trends in the meridional geostrophic transport convergence based on Sverdrup theory and the interior pycnocline transport convergence across 9°N and 9°S . Each open circle denotes a CMIP3 model marked by its model ID; the cross denotes the multimodel ensemble mean.

determined by the horizontal density gradient. Based on thermal wind balance, a lessened zonal density gradient in the pycnocline reduces the vertical shear of the meridional geostrophic flow and may result in a reduction of the geostrophic flow in the pycnocline. Indeed, Fig. 8 shows that the depth of the pycnocline base becomes shallower in the west and remains steady in the east, corresponding to a reduction of the pycnocline tilt and zonal density gradient along both 9°N and 9°S in most models. The zonal pycnocline tilt, measured by the depth difference in the pycnocline base between 135° – 155°E and 85° – 105°W along 9°N and 160°W – 180° and 80° – 100°W along 9°S , shows significant decreasing trends in five models [CGCM3.1(T47), CGCM3.1(T63), CSIRO Mk3.5, GFDL CM2.0, and MRI CGCM2.3.2; see Table 4]. In terms of the multimodel ensemble mean, the pycnocline tilt is reduced by 18.4 ± 3.2 (19.1 ± 4.1) m along 9°N (S) in the twenty-first century, in accordance with the robust weakening of the pycnocline transport in the ocean interior. The relaxation of the pycnocline tilt is likely wind driven, as a baroclinic response of the ocean to basin-scale surface wind changes. Previous theoretical studies showed that the quasi-steady response of the tropical pycnocline to a slow weakening of equatorial trade winds is characterized by both a relaxation of the pycnocline tilt and a zonal mean shoaling of the pycnocline depth (Cane and Sarachik 1981; Clarke 2010). In

CMIP3 models, the overall change of the equatorial trade winds is weakening (Fig. 5), which results in a weak pycnocline response in the eastern equatorial Pacific and a pycnocline shoaling in the western equatorial Pacific (Fig. 8). Such pycnocline responses were also noted by previous observational and multimodel intercomparison studies (Vecchi et al. 2006; Vecchi and Soden 2007). Therefore, we conclude that there is a robust weakening in the convergence of the equatorward interior pycnocline transport in the tropical Pacific Ocean under global warming, and this weakening is associated with the barotropic and baroclinic adjustment of the tropical Pacific Ocean to the changing trade winds in a warming climate.

d. Interior versus western boundary pycnocline transport

On interannual-to-decadal time scales, the variations of the pycnocline transport in the ocean interior and along the western boundary tend to partially compensate each other (Lee and Fukumori 2003; Capotondi et al. 2005). Such partial compensation is attributed to the variations of the off-equatorial wind stress curl between the tropics and subtropics (Lee and Fukumori 2003). Here, we examined the changes of the interior pycnocline transport versus the western boundary pycnocline transport to see if such partial compensation is also present on centennial time scales under greenhouse warming. Figure 9 shows the twenty-first century trends in the interior and western boundary pycnocline transport convergence across both 9°N and 9°S . The pycnocline transport convergence in the interior shows robust weakening trends in most models as described in section 3c. The changes in the western boundary pycnocline transport convergence, however, are not consistent across models, nor statistically different from zero in most models [CGCM3.1(T47), CGCM3.1(T63), CSIRO Mk3.0, GFDL CM2.0, and GFDL CM2.1]. The trend in the multimodel ensemble mean is only 0.5 ± 0.7 Sv century $^{-1}$, in contrast to a significant weakening trend of 3.5 ± 1.0 Sv century $^{-1}$ in the interior pycnocline transport convergence. As a result, the total pycnocline transport convergence shows a robust weakening similar to the interior component, with four models [CGCM3.1(T47), CGCM3.1(T63), CSIRO Mk3.5, and GFDL CM2.0] showing significant weakening trends (Table 2). Furthermore, Fig. 10 shows that at 9°N no robust compensation between the interior and western boundary pycnocline transport changes exists; and at 9°S only two models (CSIRO Mk3.5 and MRI CGCM2.3.2) show that the weakening of the interior pycnocline transport is partially compensated by a strengthening of the western boundary pycnocline transport. The multimodel ensemble-mean changes in the interior (western boundary) transport are -1.2 ± 0.4 Sv (-0.4 ± 0.4 Sv)

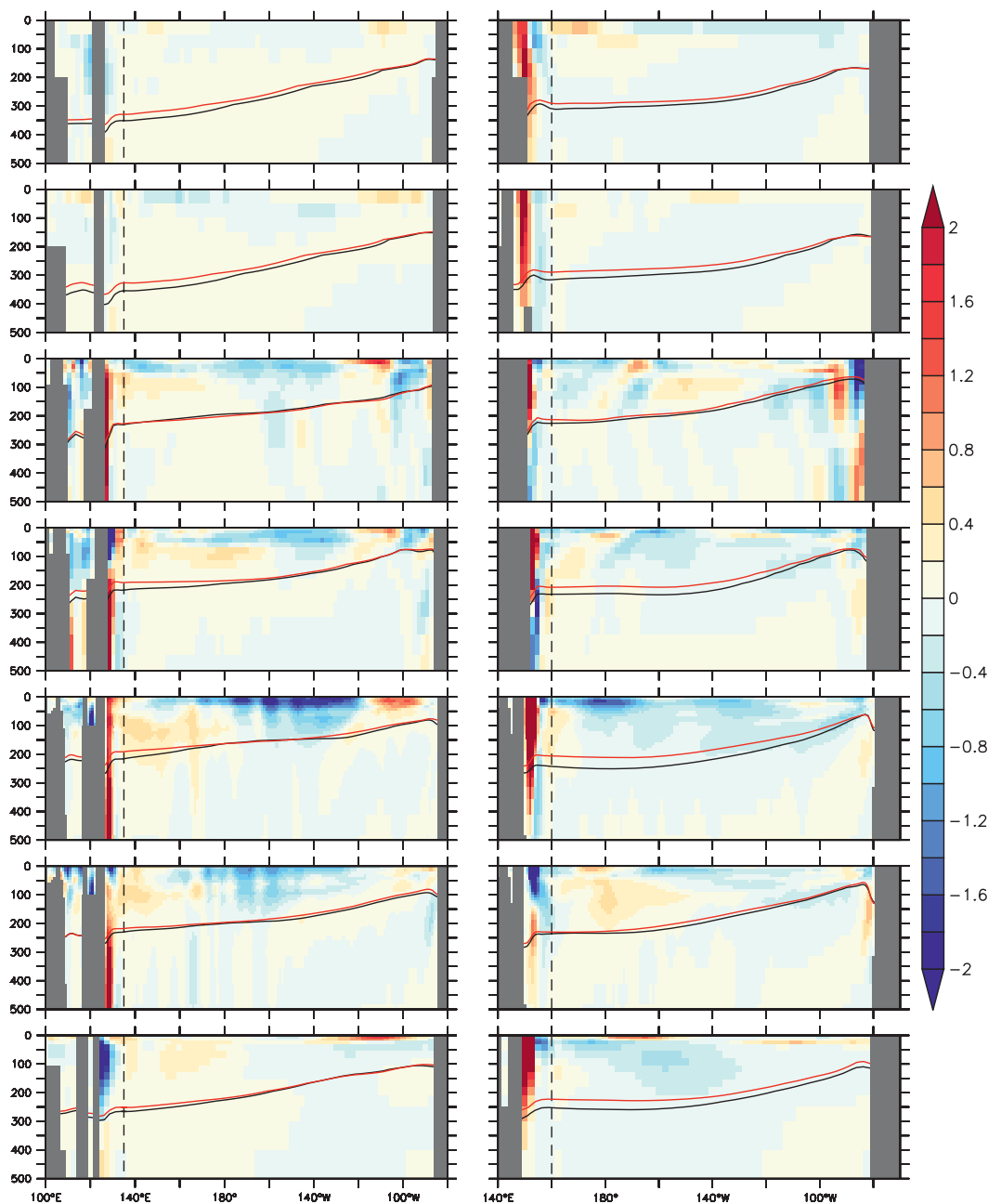


FIG. 8. Meridional velocity change (cm s^{-1}) between the first and the last 20 years of the twenty-first century in the upper Pacific Ocean (0–500 m) along (left) 9°N and (right) 9°S . The black (red) curve marks the mean pycnocline base of the first (last) 20 years of the twenty-first century. Each row corresponds to a CMIP3 model in the same order as in Table 1.

for the Northern Hemisphere and $-2.3 \pm 0.7 \text{ Sv}$ ($0.9 \pm 0.6 \text{ Sv}$) for the Southern Hemisphere. The transport changes for individual models are given in Table 3.

Our analysis showed no robust compensation between the interior and western boundary pycnocline transport changes in the twenty-first century. The changes of the pycnocline transport along the western boundary are

relatively small, and the weakening of the pycnocline transport convergence mainly takes place in the ocean interior. These results are at odds with the analysis of Luo et al. (2009) who identified a nearly complete compensation between the weakening of the interior component and the strengthening of the western boundary component of the pycnocline transport under global

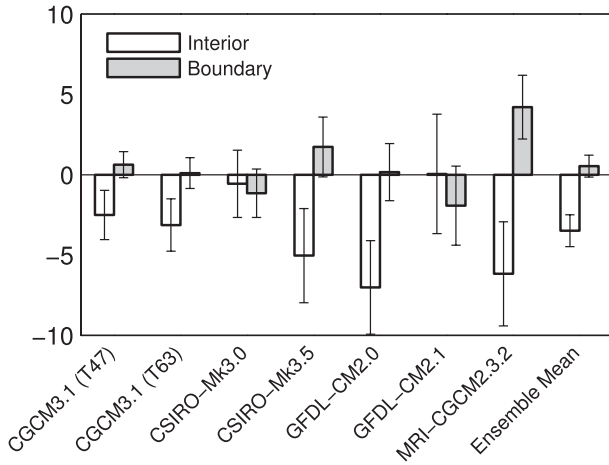


FIG. 9. Linear least squares trends (Sv century^{-1}) of the interior pycnocline transport convergence and the western boundary transport convergence across 9°N and 9°S in the twenty-first century for individual CMIP3 models and the multimodel ensemble mean. Positive (negative) values indicate strengthening (weakening) trends. Error bars indicate the 95% confidence intervals for the trends based on the F test.

warming based on a different subset of the same CMIP3 multimodel dataset. Specifically, Luo et al. (2009) found a weakening of ~ 3.2 Sv in the interior pycnocline transport convergence and a strengthening of ~ 3.0 Sv in the western boundary pycnocline transport convergence across both 9°N and 9°S between the last 50 years of the twentieth century and the last 50 years of the twenty-second century, averaged over 11 CMIP3 models. The discrepancy between our results and theirs might arise from the fact that we analyzed a different, smaller subset of CMIP3 models for a different time period. So we computed the differences in the interior and western boundary pycnocline transport convergence between the last 50 years of the twentieth century in the climate of the twentieth-century experiment (20C3M) and the last 50 years of the twenty-second century in the 720-ppm stabilization

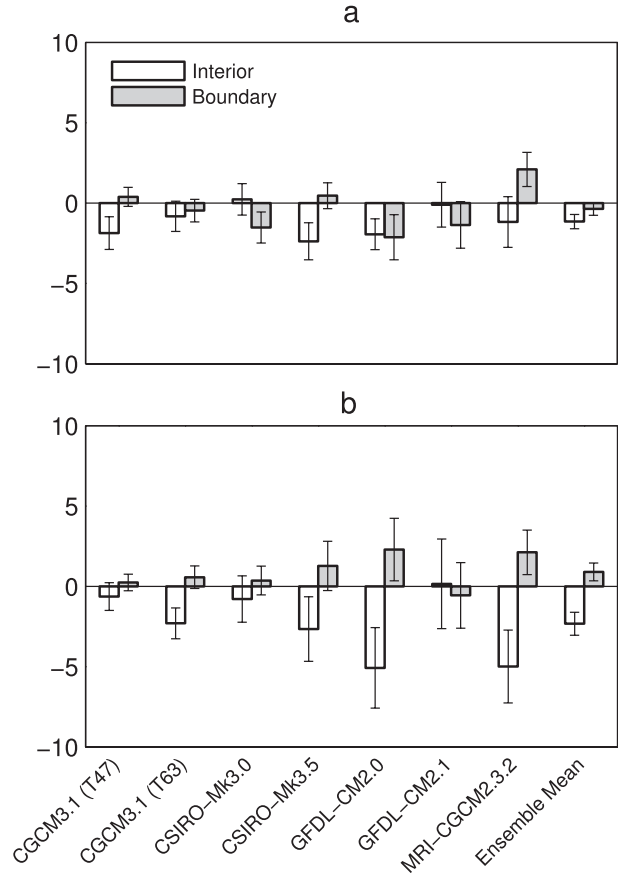


FIG. 10. As in Fig. 9, but for the transport trends at (a) 9°N and (b) 9°S separately.

experiment (SRES A1B) for five models [CGCM3.1(T63), CSIRO Mk3.0, GFDL CM2.0, GFDL CM2.1, and MRI CGCM2.3.2] that are among both our selection and that of Luo et al. (2009). The results show little difference from our twenty-first-century analysis. Only in MRI CGCM2.3.2 is the partial compensation evident between the weakening of the interior component and the strengthening of the western boundary component of the pycnocline

TABLE 3. The linear least squares trends (Sv century^{-1}) of interior (V_{IP}), western boundary (V_{BP}), and total (V_P) pycnocline transport across 9°N and 9°S for individual CMIP3 models and their ensemble mean. Positive (negative) values indicate strengthening (weakening) trends. Errors indicate the 95% confidence intervals for the trends based on the F test.

Model name	9°N			9°S		
	V_{IP}	V_{BP}	V_P	V_{IP}	V_{BP}	V_P
CGCM3.1(T47)	-1.9 ± 1.0	0.4 ± 0.6	-1.5 ± 1.0	-0.6 ± 0.9	0.2 ± 0.5	-0.2 ± 0.8
CGCM3.1(T63)	-0.8 ± 0.9	-0.5 ± 0.7	-1.3 ± 0.9	-2.3 ± 1.0	0.6 ± 0.7	-1.7 ± 0.9
CSIRO Mk3.0	0.2 ± 1.0	-1.5 ± 1.0	-1.3 ± 1.3	-0.8 ± 1.4	0.4 ± 0.9	-0.4 ± 1.5
CSIRO Mk3.5	-2.4 ± 1.2	0.5 ± 0.8	-1.9 ± 1.1	-2.7 ± 2.0	1.3 ± 1.5	-1.4 ± 1.0
GFDL CM2.0	-1.9 ± 1.0	-2.1 ± 1.4	-4.1 ± 1.5	-5.1 ± 2.5	2.3 ± 1.9	-2.8 ± 1.0
GFDL CM2.1	-0.1 ± 1.4	-1.4 ± 1.4	-1.5 ± 1.4	0.2 ± 2.8	-0.6 ± 2.0	-0.4 ± 1.2
MRI CGCM2.3.2	-1.2 ± 1.6	2.1 ± 1.1	0.9 ± 1.4	-5.0 ± 2.3	2.1 ± 1.4	-2.9 ± 1.3
Ensemble mean	-1.2 ± 0.4	-0.4 ± 0.4	-1.5 ± 0.5	-2.3 ± 0.7	0.9 ± 0.6	-1.4 ± 0.4

TABLE 4. The linear least squares trends (in m century^{-1}) of the zonal tilt of the pycnocline base (ΔD) and the depth of the pycnocline base in the western boundary region (D_{WBC}) along 9°N and 9°S in the twenty-first century for individual CMIP3 models and their ensemble mean. Positive (negative) values indicate deepening (shoaling) trends. Errors indicate the 95% confidence intervals for the trends based on the F test.

Model name	ΔD (9°N)	ΔD (9°S)	D_{WBC} (9°N)	D_{WBC} (9°S)
CGCM3.1(T47)	-27.3 ± 5.0	-20.3 ± 4.3	-24.8 ± 3.3	-23.4 ± 3.4
CGCM3.1(T63)	-32.5 ± 4.8	-30.3 ± 5.0	-37.5 ± 3.3	-31.0 ± 3.6
CSIRO Mk3.0	-2.4 ± 9.7	-1.2 ± 10.3	-14.3 ± 10.5	-20.0 ± 11.7
CSIRO Mk3.5	-22.4 ± 12.2	-19.2 ± 16.1	-31.6 ± 9.6	-33.8 ± 13.6
GFDL CM2.0	-23.7 ± 8.3	-36.7 ± 13.7	-30.4 ± 7.7	-42.3 ± 10.6
GFDL CM2.1	-3.1 ± 11.3	-4.5 ± 15.5	-7.1 ± 8.7	-12.8 ± 11.5
MRI CGCM2.3.2	-17.4 ± 6.6	-21.2 ± 8.0	-17.4 ± 4.2	-36.3 ± 7.4
Ensemble mean	-18.4 ± 3.2	-19.1 ± 4.1	-23.3 ± 2.9	-28.5 ± 3.5

transport. The multimodel ensemble-mean differences averaged over five models between two periods are -3.7 Sv for the interior pycnocline transport convergence and virtually zero for the western boundary pycnocline transport convergence. Therefore, the discrepancy between our results and those of Luo et al. (2009) cannot be explained by the different models and time periods that we used.

In principle, a measure of compensation between the variations of the pycnocline transports in the interior and along the western boundary is expected as a result of the adjustment of gyre circulation in the tropics. Based on Sverdrup theory, a strengthening (weakening) of the tropical surface wind stress curl will increase (decrease) both the poleward Sverdrup transport in the interior and the equatorward-compensating transport along the western boundary on the time scales longer than a few years when the tropical ocean is in dynamical equilibrium with the wind forcing. This results in contrasting changes in the depth-integrated, equatorward interior geostrophic transport and western boundary transport, which are mainly realized within and above the pycnocline as the circulation in the tropical Pacific is most vigorous in the upper ocean. Indeed, Fig. 8 shows that the LLWBC tends to strengthen in the twenty-first century, particularly in the Southern Hemisphere across 9°S . However, it is also evident that the depth of the pycnocline base tends to become shallower in the western boundary region. The shoaling of the pycnocline base causes a reduction in the equatorward western boundary transport *above* the pycnocline base, counteracting the strengthening of the LLWBC. The shoaling of the pycnocline base is robust across models with the multimodel ensemble-mean trends being -23.3 ± 2.9 m century^{-1} at 9°N and -28.5 ± 3.5 m century^{-1} at 9°S in the twenty-first century (Table 4).

To further illustrate the effect of the shoaling of the pycnocline base, we computed the twenty-first-century trends of the interior and western boundary pycnocline transport convergence above the mean pycnocline base

across both 9°N and 9°S (Fig. 11). The depth of the mean pycnocline base is averaged out over the first 20 years of the twenty-first century and used as a model-dependent, time-invariant lower limit of integration for the pycnocline transport. By comparing Fig. 11 with Fig. 9, it is evident that the changes of the interior pycnocline transport show little difference between two cases. The changes of the western boundary pycnocline transport, however, are very sensitive to the shoaling of the pycnocline base. In fact, in Fig. 11 there is a robust strengthening of the western boundary pycnocline transport convergence across models and the strengthening trends are significant in five models [CGCM3.1(T47), CGCM3.1(T63), CSIRO Mk3.5, GFDL CM2.0, and MRI CGCM2.3.2], which also show significant weakening trends in the interior pycnocline transport convergence. The intermodel correlation between the changes of the two components of the pycnocline transport is very strong ($r = -0.97$). In terms of the multimodel ensemble mean, the compensation is almost exact between the weakening of the interior component (-3.1 ± 1.0 Sv century^{-1}) and the strengthening of the

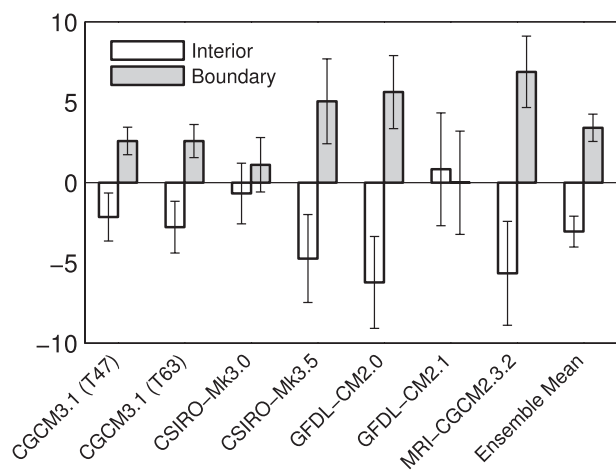


FIG. 11. As in Fig. 9, but estimated above the time-invariant mean pycnocline base.

western boundary component (3.4 ± 0.9 Sv century⁻¹) of the pycnocline transport convergence *if* the pycnocline base would not become shallower in the twenty-first century. This is similar to the results of Luo et al. (2009). However, the shoaling of the pycnocline base is a robust response among models (Fig. 8), which was probably not considered by Luo et al. (2009). Therefore, we conclude that the shoaling of the pycnocline base substantially reduces the pycnocline transport convergence along the western boundary and breaks down the compensatory behavior between the interior and western boundary pycnocline transports.

e. Indonesian Throughflow transport

Not all equatorward flow in the pycnocline convergence across 9°N and 9°S ventilates the Pacific equatorial pycnocline. Part of it exits from the western Pacific into the Indian Ocean through the ITF. The ITF transport above the pycnocline base shows a robust weakening in the twenty-first century (Table 2). The weakening trends are significant in all models except GFDL CM2.1. The multimodel ensemble-mean ITF transport above the pycnocline base weakens by 1.5 ± 0.2 Sv century⁻¹, which is very close to the difference between the changes of the surface transport divergence and pycnocline transport convergence across 9°N and 9°S (1.5 ± 1.0 Sv century⁻¹), suggesting near closure of the mass budget of the tropical Pacific above the base of the pycnocline. The reduction of ITF is consistent with the slowdown of the Walker circulation (Vecchi and Soden 2007) and associated weakening of the Pacific equatorial zonal wind stress (Fig. 4, lower panel). However, no obvious intermodel correlation is found between the changes of the ITF transport and the zonal surface wind stress over the equatorial Pacific, suggesting other processes may be responsible for the intermodel spread in the weakening of the ITF transport above the pycnocline base.

4. Summary and discussion

In this paper, we examined the twenty-first-century projected changes of the Pacific STCs in an ensemble of seven CMIP3 models. We found that there is a general tendency for the shallow meridional overturning circulation to weaken in the Northern Hemisphere and strengthen in the Southern Hemisphere under future warming. Likewise, the changes of the poleward surface-layer transport in the STCs across 9°N and 9°S also tend to be contrasting and highly correlated—weakening in the Northern Hemisphere and strengthening in the Southern Hemisphere, with the former more robust than the latter across models. They are also strongly correlated with the changes in the meridional Ekman transport across the

same latitudes, suggesting the dominant role of the local surface winds in driving the changes of the surface branches of the STCs, consistent with the STC theory (McCreary and Lu 1994; Liu 1994). The large-scale, coherent surface wind change patterns over the tropical Pacific under global warming are characterized by the weakening (strengthening) of the off-equatorial easterlies in the Northern (southern) Hemisphere and weakening of the equatorial easterlies.

The changes of the equatorward pycnocline transport in the ocean interior tend to be weakening across both 9°N and 9°S, resulting in a robust reduction of the interior pycnocline transport convergence, with a weakening trend of about -3.5 Sv century⁻¹ for the multimodel ensemble mean. This result is consistent with the single-model study by Merryfield and Boer (2005) and the multimodel study by Luo et al. (2009). The weakening of the interior pycnocline transport under global warming is associated with the relaxation of the zonal pycnocline tilt present in most models. The intermodel differences of this weakening are consistent with the wind-driven geostrophic transport changes based on Sverdrup theory. It is interesting to note that Zhang and McPhaden (2006) analyzed 14 CMIP3 models and found no significant interior pycnocline transport trend in most models during the second half of the twentieth century, suggesting that the response of the STCs in the models is not sensitive enough to greenhouse warming to be discernible in the twentieth century.

It is also found that the changes of the equatorward pycnocline transport through the western boundary are relatively minor and not consistent across models. As a result, the changes in the total pycnocline transport convergence are largely determined by the weakening of the pycnocline transport in the ocean interior. This result is consistent with the analysis by Zhang and McPhaden (2006) who found that the decadal variability of the total pycnocline transport is dominated by its interior component in 14 CMIP3 models over the last 50 years of the twentieth century. It is, however, at odds with the analysis by Luo et al. (2009) who found a robust strengthening of the western boundary pycnocline transport convergence of similar magnitude to the weakening of the interior pycnocline transport convergence, resulting in no significant change in the total pycnocline transport under global warming. It is found in our analysis that the shoaling of the pycnocline base strongly affects the changes in western boundary pycnocline transport by bringing about a transport reduction *above* the pycnocline base. If the pycnocline base were unchanged in the twenty-first century, there would be an almost exact compensation between the weakening of the interior component and the strengthening of the western boundary component of the pycnocline transport.

In addition, the ITF transport above the pycnocline base shows a robust reduction across models, which is consistent with the weakening of the easterly trade winds over the equatorial Pacific. The intermodel spread in the ITF transport change, however, cannot be adequately explained by the intermodel differences in the equatorial Pacific zonal wind stress change. Put together in terms of the multimodel ensemble-mean meridional transport changes, the response of the tropical Pacific upper-ocean mass balance to future warming in the twenty-first century involves a reduction of inflow in the pycnocline transport convergence ($2.9 \text{ Sv century}^{-1}$), and reductions of outflow of similar amounts in the surface-layer transport divergence ($1.4 \text{ Sv century}^{-1}$) and the ITF transport ($1.5 \text{ Sv century}^{-1}$), with no significant change in the water mass exchange between the pycnocline and the deep ocean.

Acknowledgments. We acknowledge the modeling groups, the Program for Climate Model Diagnosis and Intercomparison (PCMDI) and the WCRP's Working Group on Coupled Modeling (WGCM) for their roles in making available the WCRP CMIP3 multimodel dataset. Support of this dataset is provided by the Office of Science, U.S. Department of Energy. This work was partially supported by NOAA under Grant NA08OAR4320912. The authors are grateful to the anonymous reviewers for their constructive comments.

REFERENCES

- Cane, M. A., and E. S. Sarachik, 1981: The response of a linear baroclinic equatorial ocean to periodic forcing. *J. Mar. Res.*, **39**, 651–693.
- Capotondi, A., M. A. Alexander, C. Deser, and M. J. McPhaden, 2005: Anatomy and decadal evolution of the Pacific subtropical-tropical cells (STCs). *J. Climate*, **18**, 3739–3758.
- Cheng, W., M. J. McPhaden, D. Zhang, and E. J. Metzger, 2007: Recent changes in the Pacific subtropical cells inferred from an eddy-resolving ocean circulation model. *J. Phys. Oceanogr.*, **37**, 1340–1356.
- Clarke, A., 2010: Analytical theory for the quasi-steady and low-frequency equatorial ocean response to wind forcing: The tilt and warm water volume modes. *J. Phys. Oceanogr.*, **40**, 121–137.
- Delworth, T. L., and Coauthors, 2006: GFDL's CM2 global coupled climate models. Part I: Formulation and simulation characteristics. *J. Climate*, **19**, 643–674.
- DiNezio, P. N., A. C. Clement, G. A. Vecchi, B. J. Soden, B. P. Kirtman, and S. K. Lee, 2009: Climate response of the equatorial Pacific to global warming. *J. Climate*, **22**, 4873–4892.
- Godfrey, J. S., G. C. Johnson, M. J. McPhaden, G. Reverdin, and S. Wijffels, 2001: The tropical ocean circulation. *Ocean Circulation and Climate*, G. Siedler, J. Church, and J. Gould, Eds., Academic Press, 215–245.
- Gordon, H. B., and Coauthors, 2002: The CSIRO Mk3 climate system model. CSIRO Atmospheric Research Tech. Rep. 60, 134 pp.
- Gu, D., and S. G. H. Philander, 1997: Interdecadal climate fluctuations that depend on exchanges between the tropics and extratropics. *Science*, **275**, 805–807.
- Hazeleger, W., P. de Vries, and G. J. van Oldenborgh, 2001a: Do tropical cells ventilate the Indo-Pacific equatorial thermocline? *Geophys. Res. Lett.*, **28**, 1763–1766.
- , M. Visbeck, M. A. Cane, A. Karspeck, and N. Naik, 2001b: Decadal upper ocean temperature variability in the tropical Pacific. *J. Geophys. Res.*, **106**, 8971–8988.
- Held, I. M., 2001: The partitioning of the poleward energy transport between the tropical ocean and atmosphere. *J. Atmos. Sci.*, **58**, 943–948.
- , and B. J. Soden, 2006: Robust responses of the hydrological cycle to global warming. *J. Climate*, **19**, 5686–5699.
- Huang, B., and Z. Liu, 1999: Pacific subtropical-tropical thermocline water exchange in the National Centers for Environmental Prediction ocean model. *J. Geophys. Res.*, **104**, 11 065–11 076.
- Johnson, G. C., and M. J. McPhaden, 1999: Interior pycnocline flow from the subtropical to the equatorial Pacific Ocean. *J. Phys. Oceanogr.*, **29**, 3073–3089.
- Kim, S. J., G. Flato, G. Boer, and N. McFarlane, 2002: A coupled climate model simulation of the Last Glacial Maximum. Part 1: Transient multi-decadal response. *Climate Dyn.*, **19**, 515–537.
- Kleeman, R., J. P. McCreary Jr., and B. A. Klinger, 1999: Mechanism for generating ENSO decadal variability. *Geophys. Res. Lett.*, **26**, 1743–1746.
- Klinger, B. A., and J. Marotzke, 2000: Meridional heat transport by the subtropical cell. *J. Phys. Oceanogr.*, **30**, 696–705.
- Lee, T., and I. Fukumori, 2003: Interannual-to-decadal variations of tropical-subtropical exchange in the Pacific Ocean: Boundary versus interior pycnocline transports. *J. Climate*, **16**, 4022–4042.
- Liu, Z., 1994: A simple model of the mass exchange between the subtropical and tropical ocean. *J. Phys. Oceanogr.*, **24**, 1153–1165.
- , and S. G. H. Philander, 2001: Tropical-subtropical oceanic exchange pathways. *Ocean Circulation and Climate*, G. Siedler, J. Church, and J. Gould, Eds., Academic Press, 247–258.
- , —, and R. C. Pacanowski, 1994: A GCM study of tropical subtropical upper-ocean water exchange. *J. Phys. Oceanogr.*, **24**, 2606–2623.
- Lohmann, K., and M. Latif, 2005: Tropical Pacific decadal variability and the subtropical tropical cells. *J. Climate*, **18**, 5163–5178.
- Lu, P., J. P. McCreary Jr., and B. A. Klinger, 1998: Meridional circulation cells and the source waters of the Pacific equatorial undercurrent. *J. Phys. Oceanogr.*, **28**, 62–84.
- Lübbecke, J. F., C. W. Böning, and A. Biastoch, 2008: Variability in the subtropical-tropical cells and its effect on near-surface temperature of the equatorial Pacific: A model study. *Ocean Sci.*, **4**, 73–88.
- Luo, Y., L. Rothstein, and R. H. Zhang, 2009: Response of Pacific subtropical-tropical thermocline water pathways and transports to global warming. *Geophys. Res. Lett.*, **36**, L04601, doi:10.1029/2008GL036705.
- McCreary, J. P., and P. Lu, 1994: Interaction between the subtropical and equatorial ocean circulations: The subtropical cell. *J. Phys. Oceanogr.*, **24**, 466–497.

- McPhaden, M. J., and D. Zhang, 2002: Slowdown of the meridional overturning circulation in the upper Pacific Ocean. *Nature*, **415**, 603–608.
- , and —, 2004: Pacific Ocean circulation rebounds. *Geophys. Res. Lett.*, **31**, L18301, doi:10.1029/2004GL020727.
- Meehl, G. A., C. Covey, T. Delworth, M. Latif, B. McAvaney, J. F. B. Mitchell, R. J. Stouffer, and K. E. Taylor, 2007: The WCRP CMIP3 multimodel dataset. *Bull. Amer. Meteor. Soc.*, **88**, 1383–1394.
- Merryfield, W. J., and G. J. Boer, 2005: Variability of upper Pacific Ocean overturning in a coupled climate model. *J. Climate*, **18**, 666–683.
- Nonaka, M., and S. P. Xie, 2000: Propagation of North Pacific interdecadal subsurface temperature anomalies in an ocean GCM. *Geophys. Res. Lett.*, **27**, 3747–3750.
- , —, and J. P. McCreary, 2002: Decadal variations in the subtropical cells and equatorial Pacific SST. *Geophys. Res. Lett.*, **29**, 1116, doi:10.1029/2001GL013717.
- Park, W., N. Keenlyside, M. Latif, A. Ströh, R. Redler, E. Roeckner, and G. Madec, 2009: Tropical Pacific climate and its response to global warming in the Kiel climate model. *J. Climate*, **22**, 71–92.
- Rothstein, L. M., R. H. Zhang, A. J. Busalacchi, and D. Chen, 1998: A numerical simulation of the mean water pathways in the subtropical and tropical Pacific Ocean. *J. Phys. Oceanogr.*, **28**, 322–344.
- Schneider, N., A. J. Miller, M. A. Alexander, and C. Deser, 1999: Subduction of decadal North Pacific temperature anomalies: Observations and dynamics. *J. Phys. Oceanogr.*, **29**, 1056–1070.
- Schott, F. A., J. P. McCreary Jr., and G. C. Johnson, 2004: Shallow overturning circulations of the tropical-subtropical oceans. *Earth's Climate: The Ocean-Atmosphere Interaction*, C. Wang, S.-P. Xie, and J. A. Carton, Eds., American Geophysical Union, 261–304.
- Vecchi, G. A., and B. J. Soden, 2007: Global warming and the weakening of the tropical circulation. *J. Climate*, **20**, 4316–4340.
- , —, A. T. Wittenberg, I. M. Held, A. Leetmaa, and M. J. Harrison, 2006: Weakening of tropical Pacific atmospheric circulation due to anthropogenic forcing. *Nature*, **441**, 73–76.
- Xie, S. P., C. Deser, G. A. Vecchi, J. Ma, H. Teng, and A. T. Wittenberg, 2010: Global warming pattern formation: Sea surface temperature and rainfall. *J. Climate*, **23**, 966–986.
- Yukimoto, S., and A. Noda, 2002: Improvements of the Meteorological Research Institute global ocean–atmosphere coupled GCM (MRI CGCM2) and its climate sensitivity. National Institute for Environmental Studies Tech. Rep. 10, 8 pp.
- Zhang, D., and M. J. McPhaden, 2006: Decadal variability of the shallow Pacific meridional overturning circulation: Relation to tropical sea surface temperatures in observations and climate change models. *Ocean Modell.*, **15**, 250–273.